

Simple correction to band-gap problems in IV and III-V semiconductors: an improved, local first-principles density functional theory

Sujoy Datta,^{†,‡} Prashant Singh,^{*,¶} Chhanda B. Chaudhuri,[‡] Debnarayan Jana,[†]
Manoj K. Harbola,[§] Duane D. Johnson,^{*,¶,||} and Abhijit Mookerjee^{‡,⊥}

[†]*Department of Physics, University of Calcutta, Kolkata 700009, India*

[‡]*Department of Physics, Lady Brabourne College, Kolkata 700017, India*

[¶]*The Ames Laboratory, U.S. Department of Energy, Ames, Iowa 50011, USA*

[§]*Department of Physics, Indian Institute of Technology, Kanpur, 208016, India*

^{||}*Department of Materials Science & Engineering, Iowa State University, Ames, Iowa
50011, USA*

[⊥]*S. N. Bose National Centre for Basic Sciences, Salt Lake City, Kolkata 700098, India*

E-mail: prashant@ameslab.gov; ddj@iastate.edu; ddj@ameslab.gov

Abstract

Implementing van Leeuwen-Baerends (vLB) correction to local density approximation (LDA) exchange functional, we report results from a fast, efficient and first-principles full-potential N^{th} -order muffin-tin orbital (FP-NMTO) method for self-consistent (non-relativistic) calculations of electronic and structural properties of group IV and III-V semiconductors, where the more complete and compact basis set is critical in

improving the electronic and structural properties. Notably, as exemplified in Ge and GaAs, the vLB-corrected LDA within FP-NMTO results agree with experiment on the nature of the direct band-gap in GaAs and indirect ($E_{\Gamma-L}$) band-gap in Ge that most semi-local functionals get wrong. Predicted band-gap, lattice constant, and bulk modulus are in good agreement with experiments (for example, for Ge we find 0.86 eV, 5.57Å, 75 GPa vs. measured: 0.74 eV, 5.66Å, 77.2 GPa), and provide a fast means for accurate estimates of gaps and other properties after self-consistency. We also showcase its application to the structural and electronic properties of 2-dimensional h -BN and h -SiC, again finding good agreement with experiments.

Introduction

Semiconducting materials have always been of great interest due to their central role in modern electronics.¹⁻⁷ In this era of designing optimal materials, it has become essential to estimate quickly and accurately the band-gaps of such materials. Experimentally we also would benefit from an efficient computational tool for predicting band-gaps (among many other properties) prior to synthesis. We consider the problem of predicting band-gaps to be solved by a computational method that delivers an accurate result for compounds spanning the whole periodic table and is simultaneously practical to compute. Standard exchange correlation (XC) functionals to density functional theory (DFT), such as the Perdew–Burke–Ernzerhof (PBE),^{8,9} have been the backbone of DFT-based calculations for decades. Unfortunately, the unphysical self-Coulomb repulsion¹⁰ leads to a systematic underestimate of band-gaps.¹¹⁻¹³ On the other hand, hybrid functionals, such as Hartree-Fock exchange and Heyd-Scuseria-Ernzerhof functional,¹⁴ considerably reduce the Coulomb self-repulsion error¹⁵ but they substantially increase the computational time.¹⁶

Improving XC functionals in a DFT formalism remains an area of considerably active research.¹⁷⁻²³ Better and a more accurate semi-local XC functionals have been constructed by satisfying a number of exact physical behaviors,²⁴ by introducing increasingly more com-

plicated density dependence.²² In contrast, semi-empirical forms derived as corrections to the local density approximation (LDA) are fast, mathematically easy to handle and have often produce good results.^{25–31} These functionals incorporate density gradients such that the potential is asymptotically well behaved.^{27–31} For example, a van Leeuwen-Baerends (vLB) corrected²⁶ LDA has predicted band-gaps for bulk and nano-sized materials,^{27–31,34} and all were in good agreement with experimental and theoretical (hybrid-functional) values. Yet, such direct corrections to potentials fail to provide a proper DFT (i.e., total-energy functional) being not derived from a functional, and, while improved densities are found,^{31,35} they are not guaranteed. Nonetheless, accurate exact-exchange functionals with variations that approach the form enforced by vLB-LDA have appeared³² in the LibXC library,³³ but not yet explored for solids.

Despite its successes, vLB-corrected LDA, as implemented in a tight-binding linearized muffin-tin orbital (TB-LMTO) basis, underestimated band-gaps of group IV and III-V semiconductors, e.g., Ge (and indirect nature of the gap) and GaAs. As the vLB-LDA predominantly worked well, and given that basis sets play a central role in improving electronic and structural properties,^{36,37} we improve the basis set used to construct the Hamiltonian such that they are complete and compact, rather than proposing a more sophisticated XC potential, and find more accurate results.

The full-potential N^{th} -order muffin-tin orbital (FP-NMTO) method does not utilize an atomic sphere approximation (ASA), as often used in LMTO.³⁸ So, a single, compact basis set describes the entire system, including interstitial, and it is accurate whether or not the system is close-packed. For TB-LMTO, an energy-dependence basis is avoided via a Taylor’s expansion to first derivative in energy.^{39,40} For FP-NMTO, an interpolation involving higher-order derivatives is used^{41–44} and it provides a smaller and energy-independent self-consistent basis, comparable to localized Wannier functions – a prerequisite for computational speed and efficiency. Here we implement a vLB-LDA in FP-NMTO.

Theoretical detail

vLB correction in LDA

The Kohn-Sham (KS) equation transforms the interacting many-electron system to a system of non-interacting electrons moving in an effective potential due to all other electrons and ions. Using the Hohenberg-Kohn theorem, the Schrödinger's equation for many body system reduces to the so-called Kohn-Sham equation

$$\mathbf{T}_{\text{eff}}[\rho(\mathbf{r})] + \mathbf{V}_{\text{eff}}(\mathbf{r}) \Psi(\mathbf{r}) = \mathbf{E} \Psi(\mathbf{r}). \quad (1)$$

The contribution to the total energy-functional of this effective potentials is given by

$$\begin{aligned} \mathbf{E} &= - \sum_{\lambda \in \text{occ}} \int d\mathbf{r} \Psi_{\lambda}^*(\mathbf{r}) \nabla^2 \Psi_{\lambda}(\mathbf{r}) + \int d\mathbf{r} \rho(\mathbf{r}) V_{ie}(\mathbf{r}) \\ &+ \frac{1}{2} \iint d\mathbf{r} d\mathbf{r}' \frac{\rho(\mathbf{r}) \rho(\mathbf{r}')}{|\mathbf{r} - \mathbf{r}'|} + E_{xc}[\rho(\mathbf{r})] \end{aligned} \quad (2)$$

where 1st term is kinetic energy. The 2nd, 3rd, and 4th terms involve the external ion-electron [*ie*], the Hartree, and exchange-correlation [XC] contributions, respectively, which combine to provide the self-consistently determined effective potential, $V_{\text{eff}}(\mathbf{r})$, written as

$$V_{\text{eff}}(\mathbf{r}) = V_H[\rho(\mathbf{r})] + V_{ie}[\rho(\mathbf{r})] + V_{xc}[\rho(\mathbf{r})]. \quad (3)$$

Generally, $V_{xc}[\rho(\mathbf{r})]$ is given by the variation of the $E_{xc}[\rho(\mathbf{r})]$ with respect to density $\rho(\mathbf{r})$. In semi-local form, it is simplified as $E_{xc}^{\text{semi}} \simeq \int \rho(\mathbf{r}) \varepsilon_{xc}[\rho(\mathbf{r}); \nabla^{(n)} \rho(\mathbf{r})] d\mathbf{r}$ in terms of local XC energy density. The LDA, first introduced by Slater, simplifies the non-local exchange energy in terms of the local $\rho^{1/3}$ potential,⁴⁷ i.e., no gradient terms and based on homogeneous electron gas,⁴⁶ as $E_{xc}^{\text{LDA}} \simeq \int \rho(\mathbf{r}) \varepsilon_{xc}[\rho(\mathbf{r})] d\mathbf{r}$. While calculations using DFT potentials from LDA/GGA are the most successful and widespread in the last three decades, most of these calculations have resulted in significant underestimates of the band gaps of semiconductors

and insulators.

The well-established failure of many DFT and LDA results is to fail to reproduce the measured energy gaps of semiconducting material due to wrong asymptotic behavior at $r \rightarrow 0$ and $r \rightarrow \infty$ limits.²⁹ The LDA decays exponentially similar to density for finite systems, however, the potential should decay as $-1/r$, i.e., Coulomb like.⁴⁸ Becke proposed a nonlocal correction to the energy-functional and then took the functional derivative to find the exchange potential.²⁵ This gave the correct form of exchange-energy density in the asymptotic region but failed to reproduce the exact behavior for the potential. Perdew and Wang developed generalized gradient approximation (GGA) to the density.^{9,49} Later van Leeuwen and Baerends provides a similar type of correction to the LDA exchange, which improved significantly the eigenvalues for the highest-occupied orbitals of atoms.^{26,50–52} The vLB-corrected LDA potential can be written as

$$v_{xc}(\mathbf{r}) = [v_x^{LDA}(\mathbf{r}) + v_x^{vLB}(\mathbf{r})] + v_c^{LDA}(\mathbf{r}), \quad (4)$$

with

$$v_x^{vLB}(\mathbf{r}) = -\beta \rho^{1/3}(\mathbf{r}) \frac{x^2}{1 + 3\beta x \sinh^{-1}(x)} \quad (5)$$

where $x = |\nabla \rho(\mathbf{r})|/\rho^{4/3}(\mathbf{r})$ and $\beta = 0.05$. This method of gradient correction to the XC-functional is more built into the theory and thus less artificial than self-interaction-corrected (SIC) approaches.^{29,31}

Singh et al.^{29,31} recently discussed the implementation of this method in LMTO-ASA, in particular the vLB matching condition in the interstitial (an asymptotic value within a solid). Additionally, they discussed the comparison to plane-wave implementations, and why the dielectric (or work) function is not required in site-centered methods,²⁹ and how the vLB-correction potential is then able to approach results of hybrid functionals.

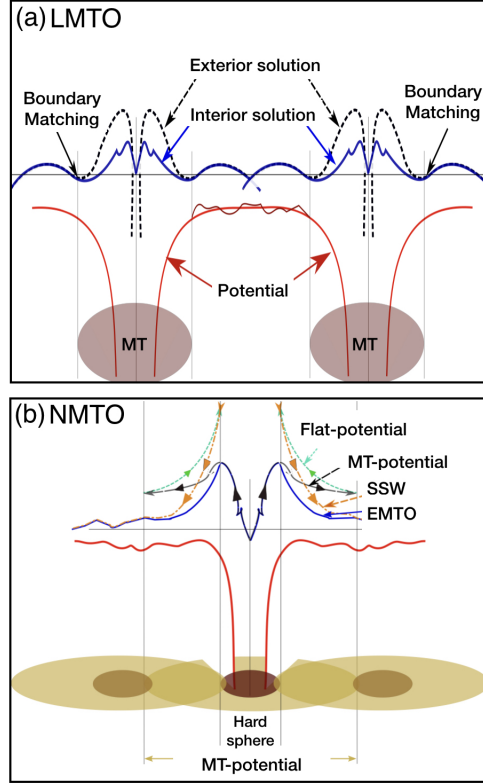


Figure 1: (Color online) Schematic of atomic spheres and corresponding potential in (a) TB-LMTO, and (b) FP-NMTO approaches.

The MT-potential and partial-wave solutions: LMTO vs NMTO

In the TB-LMTO, spheres are used to describe both the variation of electronic charge and the potential. These spheres need to be space filling with minimal (optimal) overlap ($\leq 15\%$). Overlap is essential for atomic bonding, whereas too large an overlap of charge may lead to its over-counting. The potential for a given atom is reasonably long ranged but the atomic charge density is more localized around the ion cores. Taking these ideas into account in NMTO, there are two different classes of concentric spheres: potential (MT/ASA) spheres of radius s and charge spheres (screening/hard spheres) of radius a , where $a < s$, see Fig.1(b). However, the overlap of potential spheres in NMTO can be as large as 50% so full potential approach is a pre-requisite both in ASA spheres and interstitials, see Fig.1(b).

The solutions of radial KS equations [Eq. 1] for atomic-potential φ^{as} is continued from the core of atom towards the muffin-tin surfaces at $r = s$. This is matched with the solution

for a flat part of potential (as in LMTO, this flat potential is taken as zero potential) φ^{int} , which is denoted by φ^0 . The φ^0 is valid up to the boundary of hard sphere surface ($r = a$). We normalize at the boundary of hard sphere surface (a) such that $\varphi^0|_a = 1$. The normalized wave-functions have superscript ‘‘a’’:

$$\begin{aligned}\varphi_{R,l}^a(\epsilon, r) &\equiv \frac{\varphi_{R,l}(\epsilon, r)}{\varphi_{R,l}^0(\epsilon, a_R)} \\ \varphi_{R,l}^{0a}(\epsilon, r) &\equiv \frac{\varphi_{R,l}^0(\epsilon, r)}{\varphi_{R,l}^0(\epsilon, a_R)}\end{aligned}\quad (6)$$

The $\varphi_{R,l}^{0a}(\epsilon, r)$ is matched with screened spherical waves (SSW: ψ^a) continuously but with a kink at a and truncated in the region $a_R \leq r \leq s_R$. $\varphi_{R,l}(\epsilon, r)$ is truncated outside $0 \leq r \leq s_R$. The SSWs grow outwards, which are sorted in two groups depending on the values of (R,l,m): active channels (subscript $A \equiv RL$) and passive channels (subscript $I \equiv RL$). The matching described above is for the active channels which are truncated inside hard spheres with kinks. The passive channels are substituted smoothly by φ^{as} inside hard spheres. Finally, a basis set with elements termed as Kinked Partial Waves (KPW), which are defined in all space, is formed as:

$$\begin{aligned}\phi_{Rlm}^a(\epsilon, r_R) &= [\varphi_{R,l}^a(\epsilon, r)_R - \varphi_{R,l}^{0a}(\epsilon, r_R)]Y_{l,m}(\hat{r}_R) \\ &\quad + \psi_{Rlm}^a(\epsilon, r_R)\end{aligned}\quad (7)$$

A linear combination $\sum_{RL \in A} \phi_{Rlm}^a(\epsilon_i, r_R) c_{Rlm,i}^a$ of KPWs can only be a solution of KS equation but not the individual KPWs. A kink cancellation condition can be achieved such that the kink in any hard sphere can be cancelled by the sum of the kinks from the tails of KPWs from neighboring sites. The idea is similar as the LMTO tail cancellation.

This basis set spanned by the KPWs is explicitly energy dependent. Energy dependent basis set slows down the calculation which was the problem in exact MTO (EMTO) formalism. In LMTO, energy dependence is removed by a self-consistent choice of energy ϵ_ν about

which a Taylor series expansion of basis functions are performed. The series is truncated after first order term leading to an error $\propto (\epsilon - \epsilon_\nu)^2$ in the solution of KS equation. The energy independent set of basis functions, the so called NMTO are the superposition of KPWs at a mesh of energies (calculated self-consistently) using Newton's interpolation method such that:

$$\begin{aligned}
|\chi^{0\dots N}\rangle &= \sum_{n=0}^N |\phi(\epsilon_n)\rangle L_n^{0\dots N} \\
&= |\phi[0]\rangle + |\phi[01]\rangle(E^{(0\dots N)} - \epsilon_0) + \dots + \\
&\quad |\phi[0\dots N]\rangle(E^{(N-1,N)} - \epsilon_{N-1})(E^{(0\dots N)} - \epsilon_0)
\end{aligned} \tag{8}$$

where $\phi[0] \equiv \phi(\epsilon_0)$; $\phi[01] \equiv \frac{\phi(\epsilon_0) - \phi(\epsilon_1)}{\epsilon_0 - \epsilon_1}$ are the terms in divided difference table. The error in the solution of KS equation becomes

$$\psi(\mathbf{r}) - \psi(\epsilon, \mathbf{r}) \propto (\epsilon - \epsilon_0)(\epsilon - \epsilon_1)\dots(\epsilon - \epsilon_n) \tag{9}$$

The formation of the SSWs are described in the Appendix.

Advantage of FP-NMTO over TB-LMTO

The improved basis set of FP-NMTO method is accurate, minimal and flexible. Accurate because the FP-NMTO basis solves the KS equation exactly for overlapping muffin-tin potentials. Orthonormalized FP-NMTOs are localized atom-centered Wannier functions, generated in real space with Green-function techniques, without projection from band states.⁵⁴ The TB-LMTO lacks in all above. Increased computational time is the only downside of the FP-NMTO compared to TB-LMTO.

Computational detail

We apply self-consistent FP-NMTO-vLB approach to calculate electronic properties of group IV and III-V semiconductors, in particular, Ge and GaAs. For LDA, we use the Ceperley-Alder XC functional as parameterized by Vosko-Wilk-Nusair.⁵⁵ The GGA calculations were carried out using PBE XC functional.⁸ The distinctive feature of our calculations is the use of FP-NMTO to improve the basis set with respect to TB-LMTO. The vLB correction is implemented both in TB-LMTO and FP-NMTO. We use third-order correction to the energy derivatives of wave functions ($N = 3$) within NMTO to interpolate and make the basis energy independent. We use $8 \times 8 \times 8$ k-point mesh (29 irreducible points) for Brillouin zone sampling. TB-LMTO uses the atomic-sphere approximation (ASA). The self-consistent potential converged to a difference of 10^{-6} after several tens of iterations. In calculating the lattice constant, we utilized a least square fit of our data to the Murnaghan's equation of state.⁵⁶ The calculated lattice constant is less than 0.5% overestimated with respect to experiments.^{57,58} The calculated equilibrium lattice constant is used to evaluate the bulk modulus.

Results and discussion

Bulk Germanium: In Fig. 2, we plot the band structure and total density of states (DOS) for Ge. Ge crystallizes in the diamond ($Fd\bar{3}m$) structure.⁵⁹ Two equivalent Ge's are placed at $(0, 0, 0)$ and $(1/4, 1/4, 1/4)$ in a cubic cell with empty spheres (ES) at $(-1/4, -1/4, -1/4)$ and $(1/2, 1/2, 1/2)$. Both TB-LMTO and FP-NMTO use average Wigner-Seitz radius 1.387 Å for Ge. For FP-NMTO, the hard sphere radius is 0.971 Å. The FP-NMTO-LDA gives a direct band-gap of 0.19 eV at Γ , which shows small improvement over LMTO+LDA of 0.10 eV. Treating the interstitial region in same way, use of improved basis set makes FP-NMTO better. However, if we switch to FP-NMTO-PBE, the band-gap is improved to 0.33 eV, but the nature of band-gap remains direct and more than 50% underestimated with respect to

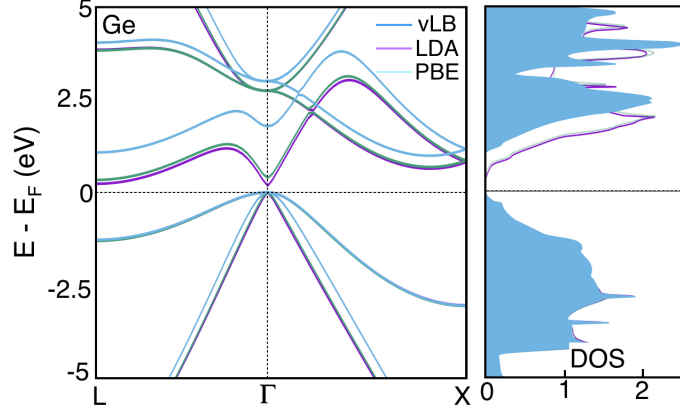


Figure 2: (Color online) For Ge, FP-NMTO band structure for LDA, PBE, and LDA-vLB functionals. The self-consistent FP-NMTO is used to obtain band structure (from $L-\Gamma-X$) and total density of states. Dispersions were aligned so that the valence band maximum is at 0 eV.

the experiments (0.74 eV). In contrast, the vLB-corrected LDA exchange within FP-NMTO opens up the band-gap to 0.86 eV. Importantly, the key point is the correct nature of band-gap, which is indirect along $\Gamma \rightarrow L$, now matches experiment. The valance bands remain almost same, whereas the conduction bands shift away from E_F .

For Ge in LDA and GGA, see Fig. 2, shows no key difference in band structure. The spaghetti of bands originated from the Ge-4s level were seen between -13 eV and -8.7 eV (see full band-structure in supplment). The Ge-4p levels with a contribution of the Ge-4s level toward the less binding energies are found at the region closer to the Fermi energy (E_F). These bands extend from -8.7 eV up to 0 eV. The conduction band mainly results from Ge-4p with minor contributions of Ge-4s atomic orbitals toward the least excited states of Ge-4d from approximately 6.30 eV and up. Some degree of degeneracy is also observed depending on which direction of the BZ is traversed: in the $L \rightarrow \Gamma$, and $\Gamma \rightarrow X$ direction. These degenerate bands belong to Ge and filled with Ge-p electrons. The Γ point has three degenerate bands; and the X point at the edge of the BZ shows two values of energies with a twofold degeneracy.

Our results show that the fundamental gap of Ge is an indirect one with the maximum of the valence band occurring at Γ and the minimum of the conduction band at the L point.²

The calculated indirect gap at equilibrium lattice constant is 0.86 eV (10% overestimation with respect to experiments). The calculated direct gap at the Γ point is ~ 2.0 eV. The LDA and GGA lead to the similar and direct gap of 0.19 eV and 0.33 eV, respectively. The LDA-vLB estimated structural properties and band-gaps are in better agreement with experiments. This also shows improvement over beyond-DFT approaches.^{5,6,60,61}

The FP-NMTO calculated DOS, compared in Fig. 2 (right-panel), for vLB-corrected shows differences both in the energy positions and in the valence bandwidths with respect to LDA and PBE. We can see a weak shoulder at -0.60 eV followed by relatively broader peaks at -1.35 , -2.25 , and -2.9 eV and a sharper peak at -4.7 eV. In the conduction bands, a small shoulder can be found at 0.9 eV followed by a peak at 2.50 eV. Other peaks can be seen at 3.2 , 4.0 , and 4.8 eV. The position of DOS-points are in closer agreement with experiments.^{2,62-65} Even though Ge is known to be an *sp* material, so the correct treatment of *3d* states is critical for accurate results. We found that major contribution of Ge-*3d* states goes to conduction bands with smaller contribution to valence states. We consider Ge-*1s2s2p* into the core,^{60,66} which leads to a better description of the band structure energies. Clearly, improving the basis set by including Ge-*3d* states into valence help achieving better energy description and fundamental (indirect) gap of Ge.

To further elaborate why vLB-corrected LDA in FP-NMTO produces better result, we plot XC-potential surface for LDA and LDA-vLB of Ge [100] plane in Fig 3. The z -axis is representing the strength of XC-potential in the range $\{0, -3\}$. As the nature of interstitial region can not be understood for the full range of XC-potential, so, we show a truncated plot along z -axis. At atomic sites, the XC-potential forms deep wells, and falls exponentially to 0 in LDA (Fig.3(a)). However, the LDA-vLB shows much slower fall than LDA (Fig.3(c)). The curvature of the XC-potential surface also improves accordingly. The plots are done at isosurface values of -0.45 eV/C for both LDA and LDA-vLB in Fig.3(b),(d). This shows that the XC-potential for Ge in LDA is much more localized at the atoms, but LDA-vLB is more spread over the cell.

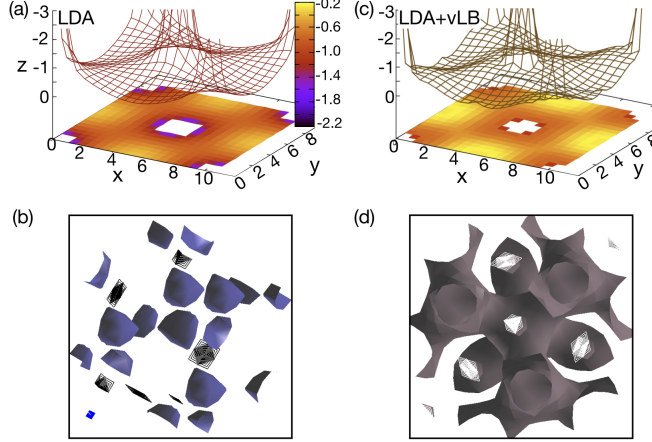


Figure 3: (Color online) For Ge, FP-NMTO XC potential (z -axis is surface range) for (a) LDA and (c) LDA+vLB in $[100]$ -plane. Potential-surface plots for (b) LDA & (d) LDA+vLB (isosurfaces of $-0.45\text{eV}/\text{\AA}$). Ge isosurface shows that XC potential is less local for LDA+vLB than LDA, which improves the band energies and gap (see Fig. 2).

Bulk Gallium-arsenide: GaAs crystallizes in the zinc-blende ($F\bar{4}3m$) structure, where Ga and As-atoms occupy $(0, 0, 0)$ and $(1/4, 1/4, 1/4)$ sites, respectively. The ES are placed to maintain the curvature of potential. We plot FP-NMTO calculated band structure and DOS in Fig. 4(a). The band-gap from LDA, PBE and LDA+vLB comes out to be 0.33 eV, 0.54 eV, and 1.43 eV, respectively. The FP-LMTO+vLB calculated band-gap of 1.43 eV shows good agreement with experimentally observed band-gap of 1.52 eV.⁶⁷ Clearly, LDA and PBE hugely underestimate the band-gap compared to LDA+vLB. Moreover, the direct (D) nature of the band-gap is also well reproduced. The band structure and DOS in Fig. 4 does not show any constant shift, which rules out any scissor operator behavior of LDA+vLB. The band structure shows larger improvement in energy levels at Γ than at X or L points. We see no change in shape of DOS except at the conduction bands near E_F and valence bands at -2.25 eV. In Fig. 4 (b),(c), the potential-energy surface for GaAs is shown along $[100]$, where overlap between the potential spheres are determined self consistently. The z -axis shows the strength of XC potential. For clarity, we show a truncated XC-potential surface in the range $\{0, -3\}$ along z -axis. We can see that at atomic sites, the XC potential forms deep well like structure, and falls exponentially to 0, which is similar to Ge. The light yellow

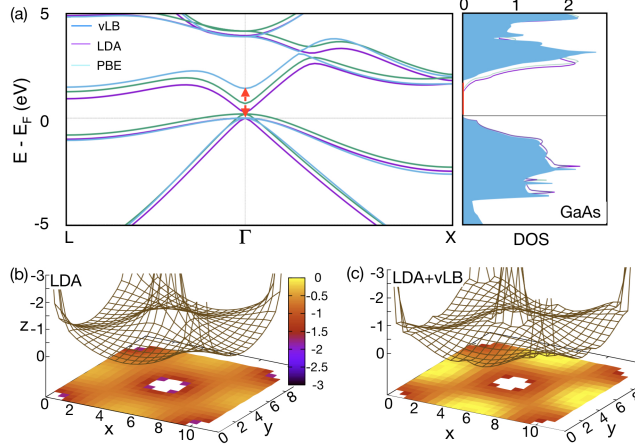


Figure 4: (Color online) For GaAs, FP-NMTO (a) band structure along L– Γ –X (left-panel) and density of states (right-panel) with LDA, PBE and LDA-vLB. The FP-NMTO-vLB band-gap (1.43 eV) shows agreement with experiment (1.52 eV).⁶⁷ We also show the XC-potential surfaces corresponding to (b) LDA and (c) LDA-vLB in [100] plane.

zone in Fig. 4(c), shows smaller interstitial contribution. This is only possible if we have smaller number of interstitial electrons than LDA (darker spots), which consequently helps correcting the energy levels in conduction band.

Table 1: FP-NMTO band-gaps for group IV and III-V materials (in eV) from LDA, PBE and LDA-vLB compared with LMTO-LDA and experiment. For LMTO-vLB see ref.[29]. I=indirect-band-gap; D=direct-band-gap.

System	a (Å)	NMTO			Expt.	LMTO LDA
		LDA	PBE	vLB		
Si	5.50	0.79(I)	0.845(I)	1.25(I)	1.17(I)	0.67
Ge	5.57	0.19(D)	0.33(D)	0.86(I)	0.74(I)	0.10
GaP	5.45	1.53(D)	1.68(D)	1.87(I)	2.32(I)	1.67
GaSb	6.00	0.26(D)	0.51(D)	0.94(I)	0.81(D)	0.08
GaAs	5.65	0.33(D)	0.54(D)	1.43(D)	1.52(D)	0.52
InAs	6.04	0.01(D)	0.04(D)	0.39(D)	0.43(D)	0.01
InSb	6.48	0.00(D)	0.02(D)	0.79(D)	0.23(D)	0.06
InP	5.85	0.5(D)	0.90(D)	1.18(D)	1.42(D)	0.60

The results for gaps of IV and III-V semiconductors are summarized in Table 1. We show that improving the basis set by using FP-NMTO and vLB-corrected LDA exchange-correlation functional yields significantly better values (with exception of InSb) and corrects the nature of the band-gap, e.g., Ge and GaP from direct to indirect (as observed).

Application to 2D materials: h -BN and h -SiC

The 2D materials, like of graphene and hexagonal boron nitride (h -BN), have drawn tremendous attention in terms of both fundamental physics and possible applications in energy-generation devices.^{68,69} Single layers of graphene and h -BN have been fabricated and found to be stable at room temperature.⁷⁰⁻⁷² Here, we exemplify the efficacy of our approach by discussing the electronic structure of 2D h -BN and SiC.⁷³⁻⁷⁵

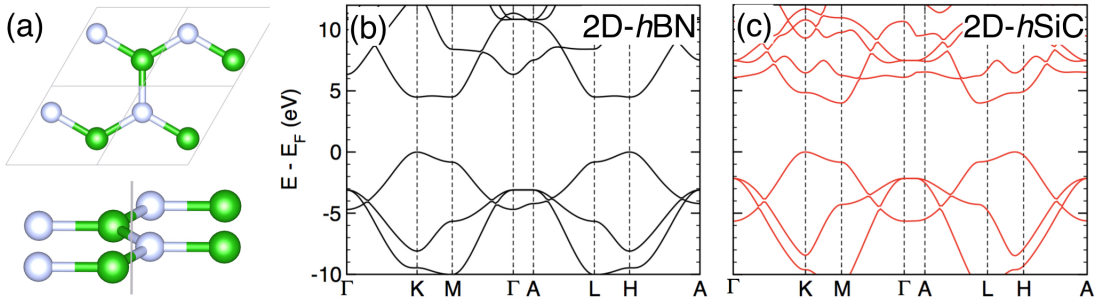


Figure 5: (Color online) For 2D h -BN and h -SiC, the (a) (001) and (101) view of the crystal structure. The FP-NMTO-vLB band structure for (b) h -BN and (c) h -SiC plotted along high-symmetry directions in the Brillouin zone. Bandgap for h -BN of ~ 4.5 eV is in good agreement with experimentally observed range (3.6 – 6 eV).⁷⁸ The band-gap for h -SiC (3.90 eV) is overestimated compared to experiment⁸³ (3 eV) but most theories find similar behavior,⁸² where, e.g., G_0W_0 overestimates (4.4 eV).⁸⁵

2D h -BN is a group III-IV binary compound displaying interesting chemical and electronic structure properties that leads to wide range of technological applications, such as protective coating, deep ultraviolet emitter, and transparent membrane.^{79,80} 2D h -BN has similar honeycomb atomic structure as graphene with a lattice mismatch of 2%,^{76,77} where each primitive cell contains a B and N atom and share total of eight electrons. Each B (N) atom forms sp^2 hybridized state with N (B), where each state forms three in-plane σ (6-electrons) and an out-of-plane π (2-electrons) bond. The NMTO-vLB energy minimized lattice constant of 2.508 Å is in good agreement with that measured (2.504 Å).⁸¹ Unlike graphene,⁶⁹ h -BN is a wide band-gap insulator.⁷⁸ The calculated band-gap of ~ 4.5 eV, in Fig. 5(b), falls within the experimentally observed band-gap range of 3.6–6 eV.⁷⁸ The nature of band gap can not be clearly stated as the band-energies of the lowest-occupied bands at

K and M are the same, i.e., a flat band along (K-M).

Similarly, 2D h -SiC is a group IV binary compound that can be viewed as graphene (2D C) or silicene (2D Si) doped with ‘Si’ or ‘C’, respectively. The honeycomb lattice of randomly but homogeneously distributed Si atoms in symmetric, semi-metallic graphene opens up a large gap. Because of its wide band-gap, h -SiC band structure has been in active study for optoelectronic applications.³⁰ Unlike the polymorphs of carbon, h -SiC is a polar material. In spite of the fact that both constituents of SiC are Group IV elements, charge is transferred from Si to C due its to higher electronegativity.

The NMTO-vLB energy minimized lattice constant of 2.62 Å is in good agreement with the measured $a=2.6\pm 0.2$ Å.^{82,83} The band-gap of 3.90 eV (indirect along K to M in Fig. 5(c)) is overestimated compared to experiment (2.96 eV).⁸³ However, a similar trend is observed in most theoretical approaches.⁸² Moreover, we found good agreement in structural behavior with experiments, while other theoretical results show significant differences, which yield a gap to be as high as 4.42 eV due to strong excitonic effects included at the G_0W_0 level of theory.⁸⁵

Conclusion

To conclude, bandgaps of semiconductors are underestimated by most semi-local exchange-correlation functionals. Here we combined two methods that directly improve bandgap predictions: (1) Using full-potential- N^{th} -order muffin-tin orbital (FP-NMTO) method, we made it self-consistent to provide a compact and complete optimal basis throughout a supercell volume – with no approximations, e.g., for interstitial regions; and (2) We implemented a van Leeuwen-Baerends (vLB) correction to the exchange potential within the FP-NMTO to provide a fast and efficient way to calculate accurate bandgaps, comparable to hybrid exchange functionals, with the speed of semilocal functionals (e.g., LDA and GGA). The combined improvement using a FP-NMTO-vLB optimal basis with a more accurate asymptotic be-

havior of the exchange hole yields much better bandgaps as well as corrected nature of the gap (e.g., indirect in Ge). In contrast to plane waves, for example, the optimal basis-set in FP-NMTO is complete for the description of the ground state and is not over-complete. The self-consistent FP-NMTO-vLB can be more effective in calculating electronic and optical properties, localized atomic orbitals (Wannier functions), or real-space tight-binding parameters for electronic-structure studies, as exemplified here for bandgaps in group IV and III-V semiconductors and 2D-hexagonal BN and SiC nanomaterials.

Acknowledgements

S.D. and A.M. would like to thank Yoshiro Nohara and O. K. Andersen for permission to modify the FP-NMTO. S.D. is thankful to I. Dasgupta for useful discussion. Research at Ames Laboratory was funded by the U.S. Department of Energy (DOE), Office of Science, Basic Energy Sciences, Materials Science and Engineering Division, which is operated for the U.S. DOE by Iowa State University under contract DE-AC02-07CH11358.

Appendix

Structure matrix in FP-NMTO

The definition of the structure matrix is important to form the Screened Spherical Waves (SSWs). In the language of NMTO, the structure matrix (S^0) of LMTO is termed as Bare Structure Matrix(B). This is found in the same way as in LMTO.

$$n_l(kr_R)Y_L(\widehat{r}_R) = \sum_{L'} j_{l'}(kr_{R'})Y_{L'}(\widehat{r}_{R'})k^{-1}B_{R'L',RL}^0(\epsilon) \quad (10)$$

$$\text{where, } B_{R'L',RL}^0 \equiv \sum_{l''} 4\pi(-1)^{\frac{-l+l'-l''}{2}} C_{LL'l''} k n_{l''}(k|\mathbf{R}-\mathbf{R}'|)Y_{l'',m''}^*(\widehat{R}-\widehat{R}') \quad (11)$$

$$\text{Gaunt coeff: } C_{LL'l''} = \int Y_L(\widehat{r})Y_{L'}^*(\widehat{r})Y_{l''(m'-m)}(\widehat{r})d\widehat{r} \quad (12)$$

If self-site terms of structure matrix is defined as $B_{R'l_m,R'l'm'}^0(\epsilon) = -ik\delta_{ll'}\delta_{mm'}$, then the one-center expansion can be written as:

$$|n^0(\epsilon, r)\rangle = |n(\epsilon, r)\rangle + k^{-1}B^0(\epsilon)|j(\epsilon, r)\rangle \quad (13)$$

The screening transformation of LMTO is made non linear in NMTO as:

$$|j^\alpha(kr)\rangle = |j(kr)\rangle - \tan \alpha_{Rlm}(\epsilon)|n(kr)\rangle \quad (14)$$

To make one center expansion similar to [eq. 13], screening transformation is found as:

$$|n^\alpha\rangle = M^\alpha|n^0\rangle = |n\rangle + k^{-1}B^\alpha|j^\alpha\rangle \quad (15)$$

Using these, the screening transformation matrix (M^α) and screened structure matrix (B^α , in LMTO it is written as S^α) is:

$$\begin{aligned} M^\alpha(\epsilon) &= 1 - \frac{\tan \alpha(\epsilon)}{k} B^\alpha(\epsilon) \text{ and } B^\alpha(\epsilon) = B(\epsilon) M^\alpha(\epsilon) \\ B^\alpha(\epsilon)^{-1} &= B(\epsilon)^{-1} \frac{\tan \alpha(\epsilon)}{k} \end{aligned} \quad (16)$$

where, $k^{-1} \tan \alpha = k^{-1} \tan \alpha_{RL} \delta_{RR'} \delta_{LL'}$ is diagonal and $B^\alpha(\epsilon), B(\epsilon)$ are Hermitian.

Screened Spherical Waves (SSW)

The SSWs are envelop functions produced as a superposition of the Neumann's functions as:

$$|n^\alpha(\epsilon)\rangle = M^\alpha(\epsilon) |n^0(\epsilon)\rangle \quad (17)$$

The background phase shifts (α) are equal to the real phase shifts (η) in case of inactive channels.

$$\begin{aligned} |j_I^\alpha(kr)\rangle &= |j_I(kr)\rangle - \tan \eta_I(\epsilon) |n(kr)\rangle \\ &= -\tan \eta_I(\epsilon) |\varphi_I^0(\epsilon, r)\rangle \end{aligned} \quad (18)$$

These screened envelop functions for inactive channels are set in a way that for inactive channels, these φ_I^0 can be substituted smoothly by the regular solutions [eq. 6] φ_I^a . This process is called "downfolding" and after this substitution the screened envelop functions become the Screened Spherical waves ψ . The MTOs are formed by the SSWs of the remaining active channels.

References

- (1) H. Droge, M. Nagelstrasser, J. Numberger, W. Faschinger, A. Fleszar, and H.-P. Steinrumck, *Surf. Sci.* **454**, 477 (2000).
- (2) E. Landemark, C.J. Karlsson, L.S.O. Johansson, and R. I. G. Uhrberg, *Phys. Rev. B* **49**, 16523 (1994).
- (3) J.A. Stroscio, R.M. Feenstra, and A.P. Fein, *Phys. Rev. Lett.* **57**, 2579 (1986).
- (4) R.M. Feenstra, J.A. Stroscio, and A.P. Fein, *Surf. Sci.* **181**, 295 (1987).
- (5) W. Ku, and A.G. Eguiluz, *Phys. Rev. Lett.* **89**, 126401 (2002).
- (6) P.V. Smith, M. Hermanowicz, G.A. Shah, and M.W. Radny, *Computational Materials Science* **54**, 37 (2012).
- (7) H. Yutaka, I. Kojiro, Y. Akira, and K. Makoto, *Jpn. J. Appl. Phys.* **48**, 04C125 (2009).
- (8) J.P. Perdew, K. Burke, and M. Ernzerhof, *Phys. Rev. Lett.* **77**, 3865 (1996).
- (9) K. Burke, J. P. Perdew, and Y. Wang, in *Electronic Density Functional Theory*, edited by M. P. Das, G. Vignale, and J. F. Dobson (Plenum, New York, 1997).
- (10) J.P. Perdew, and A. Zunger, *Phys. Rev. B* **23**, 23, 5048 (1981).
- (11) J.P. Perdew, and M. Levy, *Phys. Rev. Lett.* **51**, 1884 (1983).
- (12) L.J. Sham, and M. Schlüter, *Phys. Rev. Lett.* **51**, 1888 (1983).
- (13) P. Mori-Sanchez, A.J. Cohen, and W. Yang, *Phys. Rev. Lett.* **100**, 146401 (2008).
- (14) J.K. Perry, J. Tahir-Kheli, and W.A. Goddard, *Phys. Rev. B* **63**, 144510 (2001).
- (15) A.V. Krukau, O.A. Vydrov, A.F. Izmaylov, and G.E. Scuseria, *J. Chem. Phys.* **125**, 224106 (2006).

- (16) J.M. Crowley, J.T. Kheli, and W.A. Goddard, *J. Phys. Chem. Lett.* **7**, 1198 (2016).
- (17) S. Kümmel, and L. Kronik, *Rev. Mod. Phys.* **80**, 3 (2008).
- (18) K. Burke, and *J. Chem. Phys.* **136**, 150901 (2012).
- (19) W. Yang, P. Mori-Sanchez, and A.J. Cohen, *AIP Conf. Proc.* **1504**, 605 (2012).
- (20) A.D. Becke, *J. Chem. Phys.* **140** (18), 18A301 (2014).
- (21) R.O. Jones, *Rev. Mod. Phys.* **87**, 897 (2015).
- (22) H.S. Yu, S. L. Li, and D.G. Truhlar, *J. Chem. Phys.* **145**, 130901 (2016).
- (23) J.P. Perdew, A. Ruzsinszky, J. Tao, V.N. Staroverov, G.E. Scuseria, and G.I. Csonka, *J. Chem. Phys.* **123**, 062201 (2005).
- (24) M.G. Medvedev, I.S. Bushmarinov, J. Sun, J.P. Perdew, and K.A. Lyssenko, *Science* **355**, 49 (2017).
- (25) A.D. Becke, *Phys. Rev. A* **38**, 3098 (1988).
- (26) R. van Leeuwen and E.J. Baerends, *Phys. Rev. A* **49**, 2421 (1994).
- (27) P. Singh, M.K. Harbola, B. Sanyal and A. Mookerjee, *Phys. Rev. B* **87**, 235110 (2013).
- (28) P. Singh, M.K. Harbola, and A. Mookerjee, *Calculation of band-gaps for bulk-and nano-materials using Harbola-Sahni and van Leeuwen-Baerends Potentials*, in *Modeling, Characterization, and Production of Nanomaterials*, Ed. V.K. Tewary, and Y. Zhang (Woodhead Publishing, Massachusetts 2015), Edition 1, Vol. 1, pp. 407-418.
- (29) P. Singh, M.K. Harbola, M. Hemanadhan, A. Mookerjee D.D. Johnson, *Phys. Rev. B* **93**, 085204 (2016).
- (30) B. Sadhukhan, P. Singh, A. Nayak, S. Datta, D.D. Johnson, and A. Mookerjee, *Phys. Rev. B* **96**, 054203 (2017).

- (31) P. Singh, M.K. Harbola, and D.D. Johnson, *J. Phys.: Condens. Matter* **29**, 424001 (2017).
- (32) T. Chachiyo and H. Chachiyo, arXiv:1706.01343 (2017).
- (33) M.A.L. Marques, M. J. T. Oliveira, and T. Burnus, *Comput. Phys. Commun.* **183**, 2272 (2012).
- (34) M. Rahaman, P. Singh, A. Mookerjee, and M.K. Harbola, *The band-gap problem: An approach using the modified density functional theory and the Harbola-Sahni exchange potential*, in *Simulation and Characterization of the Advanced Materials Edition*, Ed. S. Kumar, (Transworld Research Network, 2010), Edition 1, Ch. 2, pp. 13-26.
- (35) J.P. Perdew et al., *Proc. Natl. Acad. Sci. USA* **114** (11), 2801 (2017).
- (36) O.K. Andersen, and T. Saha-Dasgupta, *Phys. Rev. B* **62**, R16 219 (2000).
- (37) H. Takeda, A. Chutinan, and S. John, *Phys. Rev. B* **74**, 195116 (2006).
- (38) Y. Nohara, O.K. Andersen, *Phys. Rev. B.* **94**, 101103 (2016).
- (39) H.L. Skriver, *The LMTO Method* (Springer, New York, 1984).
- (40) O.K. Andersen, *Phys. Rev. B* **12**, 3060 (1975).
- (41) O.K. Andersen, O. Jepsen, and G. Krier *Lectures in Methods of Electronic Structure Calculations, Eds.: V. Kumar, O.K. Andersen, A. Mookerjee* (World Sci. Publ. Co., Singapore, 1994).
- (42) L. Vitos *Computational Quantum Mechanics for Materials Engineers; The EMTO Method and Applications* (Springer, London, 2007).
- (43) O.K. Andersen, C. Arcangeli, R.W. Tank, T. Saha-Dasgupta, G. Krier, O. Jepsen, I. Dasgupta *Tight-Binding Approach to Computational Materials Science, Eds. L. Colombo, A. Gonis, P. Turchi* (MRS Symposium Proceedings Series, vol 491, 1998).

- (44) W.R.L. Lambrecht, and O.K. Andersen, Phys. Rev. B **34**, 2439 (1986).
- (45) M.K.Y. Chan, and G. Ceder, Phys. Rev. Lett. **105**, 196403 (2010).
- (46) U. von Barth, and L. Hedin, J. Phys. Chem. **5**, 1629 (1972).
- (47) J.C. Slater, Phys. Rev. **81**, 385 (1951).
- (48) C.O. Almbladh and U. von Barth, Phys. Rev. B **31**, 3231(1985).
- (49) J.P. Perdew, and Y. Wang, Phys. Rev. B **33**, 8800 (1986).
- (50) M.K. Harbola, and V.K. Sahni, Phys. Rev. Lett. **62**, 489 (1989).
- (51) M.K. Harbola, and V.K. Sahni, Int. J. Quantum Chem. **24**, 569 (1990).
- (52) A. Banerjee, and M.K. Harbola, Phys. Rev. A **60**, 3599(1999).
- (53) J. Choi, E.-H. Chang, D.M. Anstine, M. A.-E. Madjet, H.S. Chakraborty, Phys. Rev. A **95**, 023404 (2017)
- (54) M.W. Haverkort, M. Zwierzycki, and O.K. Andersen, Phys. Rev. B **85**, 165113 (2012).
- (55) S.H. Vosko, L. Wilk and M. Nusair, Can. J. Phys. **58** (8), 1200 (1980).
- (56) F.D., Murnaghan, Proc. Natl. Acad. Sci. USA **30**, 244 (1944).
- (57) I.N. Remediakis, and E. Kaxiras, Phys. Rev. B **59**, 5536 (1999).
- (58) *Semiconductos. Physics of Group IV elements and III-V Compounds*, Ed. K.H. Hellwege and O. Madelung, Landolt- Bornstein, New Series, Group III, Vol. 17,(Springer, Berlin, 1982).
- (59) J.S. Kasper, and S.M. Richards, Acta Crystallographica **17**, 752 (1964).
- (60) M. Rohlfing, P. Krüger, and J. Pollmann, Phys. Rev. B **48**, 17791 (1993).

- (61) M.S. Hybertsen, and S.G. Louie, Phys. Rev. B **34**, 5390 (1986).
- (62) D.E. Eastman, W.D. Grobman, J.L. Freeouf, and M. Erbudak, Phys. Rev. B **9**, 3473 (1974).
- (63) D. Straub, L. Ley, and F.J. Himpsel, Phys. Rev. B **33**, 2607 (1986).
- (64) D.A. Muzychenko, S.V. Savinov, V.N. Mantsevich, N.S. Maslova, V.I. Panov, K. Schouteden, and C.V. Haesendonck, Phys. Rev. B **81**, 035313 (2010).
- (65) W.B. Jackson, J.E. Northrup, J.W. Allen, and R.I. Johnson, Phys. Rev. Lett. **56**, 1187 (1986).
- (66) E.L. Shirley, X. Zhu, and S.G. Louie, Phys. Rev. Lett. **69**, 2955 (1992).
- (67) P. Villars, and K. Cenzual, *GaAs Crystal Structure: Datasheet* from “PAULING FILE Multinaries” in SpringerMaterials (Springer-Verlag Berlin Heidelberg, 2012).
- (68) A.H.C. Neto, F. Guinea, N.M.R. Peres, K.S. Novoselov, and A.K. Geim, Rev. Mod. Phys. **81**, 109 (2009).
- (69) A.K. Geim, and K.S. Novoselov, Nat. Mater. **6**, 183 (2007).
- (70) K.S. Novoselov, D. Jiang, F. Schedin, T.J. Booth, V.V. Khotkevich, S.V. Morozov, and A.K. Geim, Proc. Natl. Acad. Sci. U.S.A. **102**, 10451 (2005).
- (71) J.C. Meyer, A.K. Geim, M.I. Katsnelson, K.S. Novoselov, T.J. Booth, and S. Roth, Nature **446**, 60 (2006).
- (72) M.H. Gass, U. Bangert, A.L. Bleloch, P. Wang, R.R. Nair, and A.K. Geim, Nat. Nanotechnol. **3**, 676 (2008).
- (73) P. Nath, S. Chowdhury, D. Sanyal and D. Jana, Carbon **73**, 275 (2014).
- (74) . S. Chowdhury, and D. Jana, Reports On Progress in Physics **79**, 126501 (2016)

- (75) .D. Jana, P. Nath and D. Sanyal, *Modification of electronic structure of graphene by Boron and Nitrogen doping*, in Graphene Science Handbook: Nanostructure and Atomic Arrangement Edited by M. Aliofkhazraei, N. Ali, W.I. Milne, C.S. Ozkan, S. Mitura, J.L. Gervasoni, (CRC Publications, Taylor and Francis, ISBN 9781466591370, 2016), pp. 231.
- (76) Z. Liu *et al.*, Nature Nanotech. **8**, 119 (2013).
- (77) C.R. Dean, A.F. Young, I. Meric, C. Lee, L. Wang, S. Sorgenfrei, K. Watanabe, T. Taniguchi, P. Kim, K.L. Shepard, and J. Hone, Nature Nanotech **5**, 772 (2010).
- (78) Y. Kubota, K. Watanabe, O. Tsuda, and T. Taniguchi, Science **317**, 932 (2007).
- (79) A. Hsu, X. Jia, S.M. Kim, Y. Shi, M. Hofmann, D. Nezich, J.F. Rodriguez-Nieva, M. Dresselhaus, T. Palacios, and J. Kong, Nano Lett. **12**, 161 (2012).
- (80) S. Dai *et al.* Nature Nanotech. **14**, 421 (2015).
- (81) V.L. Solozhenko, A.G. Lazarenko, J.-P. Petitet, and A.V. Kanaev, Journal of Physics and Chemistry of Solids **62**, 1331 (2001)
- (82) M.S. Sharif Azadeh, A. Kokabi, M. Hosseini, and M. Fardmanesh, Micro & Nano Letters **6**, 582 (2011).
- (83) S.S. Lin, J. Phys. Chem. C **116**, 3951 (2012).
- (84) E. Bekaroglu, M. Topsakal, S. Cahangirov, and S. Ciraci, Phys. Rev. B **81**, 075433 (2010).
- (85) H.C. Hsueh, G.Y. Guo, and S.G. Louie, Phys. Rev. B **84**, 085404 (2011).